Published in final edited form as:
Biochem J. ; 426(3): 281–292. doi:10.1042/BJ20091351.

Molecular mechanism of elongation factor 1A inhibition by a *Legionella pneumophila* glycosyltransferase

Ramon Hurtado-Guerrero[*,1], **Tal Zusman**[†], **Shalini Pathak**[*], **Adel F. M. Ibrahim**[‡], **Sharon Shepherd**[*], **Alan Prescott**[§], **Gil Segal**[†], and **Daan M. F. Van AALTEN**[*,1]

[*]Division of Molecular Microbiology, College of Life Sciences, University of Dundee, Dundee DD1 5EH, Scotland, U.K.

[†]Molecular Microbiology and Biotechnology, Life Sciences, Tel Aviv University, Tel Aviv, Israel

[‡]DNA Manipulation Team, College of Life Sciences, University of Dundee, Dundee DD1 5EH, Scotland, U.K.

[§]Division of Cell Biology and Immunology, College of Life Sciences, University of Dundee, Dundee DD1 5EH, Scotland, U.K.

Abstract

Legionnaires' disease is caused by a lethal colonization of alveolar macrophages with the Gram-negative bacterium *Legionella pneumophila*. *Lp*GT (*L. pneumophila* glucosyltransferase; also known as Lgt1) has recently been identified as a virulence factor, shutting down protein synthesis in the human cell by specific glucosylation of EF1A (elongation factor 1A), using an unknown mode of substrate recognition and a retaining mechanism for glycosyl transfer. We have determined the crystal structure of *Lp*GT in complex with substrates, revealing a GT-A fold with two unusual protruding domains. Through structure-guided mutagenesis of *Lp*GT, several residues essential for binding of the UDP-glucose-donor and EF1A-acceptor substrates were identified, which also affected *L. pneumophila* virulence as demonstrated by microinjection studies. Together, these results suggested that a positively charged EF1A loop binds to a negatively charged conserved groove on the *Lp*GT structure, and that two asparagine residues are essential for catalysis. Furthermore, we showed that two further *L. pneumophila* glycosyltransferases possessed the conserved UDP-glucose-binding sites and EF1A-binding grooves, and are, like *Lp*GT, translocated into the macrophage through the Icm/Dot (intracellular multiplication/defect in organelle trafficking) system.

Keywords

elongation factor 1A (EF1A); glucosyl transferase; *Legionella pneumophila*; microinjection; site-directed mutagenesis; protein structure

[1]Correspondence may be addressed to either of these authors (R.HurtadoGuerrero@dundee.ac.uk or dmfvanaalten@dundee.ac.uk). .

The structural co-ordinates reported will appear in the Protein Data Bank under accession codes 2WZF and 2WZG.

AUTHOR CONTRIBUTION

Ramon Hurtado-Guerrero and Daan van Aalten initiated the project. Ramon Hurtado-Guerrero, Shalini Pathak, Alan Prescott and Gil Segal designed the type of experiments to be performed. Ramon Hurtado-Guerrero, Tal Zusman, Shalini Pathak, Adel Ibrahim, Sharon Shepherd and Alan Prescott performed the experiments. Ramon Hurtado-Guerrero, Alan Prescott, Gil Segal and Daan van Aalten interpreted the results. Ramon Hurtado-Guerrero and Daan van Aalten wrote the manuscript.

Europe PMC Funders Author Manuscripts

INTRODUCTION

Over the past decade several studies have reported fascinating examples of pathogenic bacteria employing glycosyltransferases secreted into the human cell to control specific signal transduction pathways/cellular processes. For instance, the GT44 family {as annotated in the CAZY (carbohydrate-active enzyme) database; [1]} TcdA (*Clostridium difficile* toxin A) and TcdB (*C. difficile* toxin B) glycosyltransferase enzymes cause pseudomembranous colitis and antibiotic-associated diarrhoea by monoglucosylating Rho-family GTPases (such as Rho at Thr^{37}, Rac at Thr^{35} and Cdc42) leading to the disruption of binding to GDIs (guanosine nucleotide dissociation inhibitors), inhibition of activation by GEFs (guanine-nucleotide-exchange factors), inhibition of the membrane–cytoplasm cycle and inhibition of the GTPase-active form [2-5]. Another bacterial glucosyltransferase, *Lp*GT (*Legionella pneumophila* glucosyltransferase, also called Lgt1 or lpg1368) has been suggested to be involved in pathogenesis [6,7]. *L. pneumophila* is an intracellular opportunistic Gram-negative pathogen able to proliferate within human alveolar macrophages [8] and is the causative agent of Legionnaires' disease [9]. This bacterium, once engulfed by macrophages, is able to replicate in vacuoles/phagosomes independently of the classical endolysosomal pathway [8,10], until nutrient levels decline, leading to activation of the Icm/Dot (intracellular multiplication/defect in organelle trafficking) type IV secretion system that releases several virulence factors [11]. At this stage, flagellated bacteria are released and infect new host cells. *Lp*GT, annotated as a family GT88 glucosyltransferase in the CAZY database [1], was discovered to be a virulence factor, glucosylating Ser^{53} of hEF1A (human elongation factor 1A) by a retaining mechanism [12], leading to inhibition of ribosomal translation and consequently cell death [7]. However, the molecular mechanisms of glycosyl transfer and recognition of hEF1A are not understood.

In the present paper, we report the crystal structure of *Lp*GT, which reveals a GT-A fold, demonstrating how the enzyme interacts with UDP-glucose. Through mutagenesis we identified residues important for catalysis and hEF1A recognition. We studied the effect of the residues on virulence, through microinjection studies, revealing that a positively charged hEF1A loop probably interacts with a conserved binding groove on *Lp*GT. We also showed that two recently described apparent *Lp*GT homologues, Lgt3 (*L. pneumophila* glucosyltransferase 3; also known as LegC5) and Lgt2 (*L. pneumophila* glucosyltransferase 2; also known as LegC8), possess a conserved UDP-glucose-binding site and hEF1A-binding groove and are, like *Lp*GT, translocated through the Icm/Dot machinery, killing mammalian cells through induction of apoptosis.

EXPERIMENTAL

Cloning, mutagenesis and purification of *L. pneumophila* glucosyltransferases

Two open reading frames (lpg1368 and lpl1319; TrEMBL accessions Q5ZVS2 and Q5WWY0) encoding *LppGT* (*Lp*GT from strain *Philadelphia*-1; ATCC 33152) and *Lpl*GT (*Lp*GT from strain *Lens*) respectively were amplified by PCR from genomic DNA extracted from the respective strains using the primers listed in Supplementary Table S1 (available at http://www.BiochemJ.org/bj/426/bj4260281add.htm), and the PCR products were cloned directly into the bacterial expression vector pGEX6P1 (GE Healthcare).

Site-directed mutagenesis was carried out following the QuikChange® site-directed mutagenesis protocol (Stratagene), using the KOD HotStart DNA polymerase (Novagene). The resulting plasmid, pGEX6P1-*lpgt Philadelphia* strain, also referred to as wild-type, was used as template for introducing the following single amino-acid changes by site-directed mutagenesis: D246A, D248A, D246A-D248A, N293A, E445A, E446A, Y454A, N499A

and S519A. FLAG tags were also incorporated by site-directed mutagenesis. All plasmids were verified by sequencing.

The plasmids were transformed into *Escherichia coli* BL21(DE3) pLysS cells and grown at 37°C until reaching an attenuance of 0.6 at 600 nm, after which the expression of the protein was induced with 0.2 mM IPTG (isopropyl β-D-thiogalactoside) at room temperature (23°C) for an overnight incubation. The cells were harvested by centrifugation at 3480 ***g*** for 30 min and resuspended in buffer A [25 mM Tris/HCl, pH 8.5, 250 mM NaCl and 4 mM DTT (dithiothreitol)], containing lysozyme (1 mg/ml; Sigma–Aldrich), DNAse (0.1 mg/ml; Sigma–Aldrich) and protease inhibitors (1 tablet in 50 ml of lysis buffer; Roche). The cells were disrupted by a continuous-flow cell disruptor (Constant Systems) at a pressure of 30 psi (1 psi=6.9 kPa) and centrifuged at 19000 ***g*** at 4°C for 30 min. The supernatant was incubated at 4°C with glutathione–Sepharose 4B beads (Amersham Biosciences), which had been equilibrated with buffer A for 2 h. Then the proteins were cleaved overnight at 4°C with PreScission (GE Healthcare) protease. The supernatant containing the proteins was concentrated prior to gel-filtration chromatograpy on a Superdex 75 XK26/60 column using an AKTA Prime system (GE Healthcare). The column was equilibrated with two column volumes of buffer B (25 mM Tris/HCl, pH 8.5, 150 mM NaCl and 4 mM DTT). The purification was run at a flow rate of 1 ml/min and 3 ml fractions were collected. The eluted peak containing the protein was concentrated and used for crystallization trials, or frozen with 25% glycerol at −80°C.

Enzymology

Mammalian cell lysates were prepared from HEK (human embryonic kidney)-293 cells. Cells were harvested by centrifugation at 3480 ***g*** for 30 min and resuspended in cold lysis buffer C [50 mM Tris/HCl, pH 7.5, 0.1 mM EGTA, 1 mM EDTA, 1% (v/v) Triton X-100, 1 mM Na_3VO_4, 50 mM NaF, 5 mM sodium pyrophosphate, 0.27 M sucrose and 0.1% 2-mercaptoethanol] with 1× protease inhibitor cocktail (Roche). Protein concentrations of the lysates were determined using the Bradford method [13]. Glucosylation reactions were performed in 20 μl volumes consisting of buffer D (20 mM Tris/HCl, pH 7.5, 150 mM NaCl and 1 mM $MnCl_2$), 7 μM recombinant glucosyltransferase, 50 μg of crude cell extract and 2.5 μM UDP-[^{3}H]glucose (American Radiolabeled Chemicals). The mixture was incubated at 37°C for 3 h. The reaction was stopped by the addition of LDS (lithium dodecyl sulfate) sample buffer and heated at 100°C for 3 min. The samples were then subjected to SDS/PAGE (stacking and resolving gels at 4% and 12% respectively). Gels were stained with 0.1% Coomassie Brilliant Blue in 40% (v/v) methanol and 10% (v/v) acetic acid for 60 min and destained overnight with 10% (v/v) acetic acid and 30% (v/v) methanol. Incorporation of [^{3}H]glucose in proteins was visualized by treatment with EN^{3}HANCE (Perkin Elmer) for 30 min, followed by fluorography using X-Omat film (Kodak). Densitometry was quantified using Aida analysis software.

Binding of UDP-glucose to wild-type and mutant *Lpp*GT was analysed by ligand-induced quenching of intrinsic tryptophan fluorescence. Fluorescence measurements were carried out with a Varian Cary Eclipse fluorescence spectrophotometer equipped with a thermostatted cuvette holder equilibrated at 25°C. Emission spectra were recorded from 300–400 nm upon excitation at 295 nm. Excitation and emission slits were opened to 10 nm and 20 nm respectively and the spectra were recorded at a scan speed of 9–60 nm/min. Standard reaction mixtures contained 1 μM of *Lp*GT in 25 mM Tris/HCl, pH 7.5, 150 mM NaCl and 1 mM $MnCl_2$ in a final volume of 1 ml. After pre-incubation for 10 min at 25°C within the cuvette holder, aliquots of UDP-glucose were added to the mixture (the total added volume did not exceed 2% of the total volume). The emission spectrum was recorded after each addition following mixing and 5 min incubation. All of the spectra were corrected for the

background emission signal from both the buffer and the unbound UDP-glucose and repeated in triplicate. The equilibrium dissociation constant was obtained from fitting the fluorescence intensity data to the standard single-site binding equation with the software GraFit (Erithacus Software).

Microinjection

HeLa cells [14] were seeded on to 13-mm glass coverslips and allowed to settle overnight. The cells were then microinjected with 30 μM protein containing Texas Red-conjugated dextran (to localize the injected cells) in injection buffer E (100 mM glutamic acid, pH 7.2 with citric acid [15], 140 mM KOH, 1 mM $MgSO_4$ and 1 mM DTT) as described previously [16]. The number of injection attempts were counted by the microinjector (Eppendorf) and recorded. Following incubation for 48 h, the cells were fixed in 4% (w/v) PFA (paraformaldehyde) in PBS and counterstained with DAPI (4′,6-diamidino-2-phenylindole) to distinguish apoptotic nuclei. The number of surviving cells (both those still adherent to the coverslip and rounded-up cells) were then counted and expressed as a percentage of the number of injection events. Note that not all injection events were successful and that after 48 h unperturbed cells would divide such that the final counts could exceed 100%.

Microscopy

HeLa cells were injected as described above with FLAG-tagged proteins and, following incubation for 24 h, the cells were fixed in 4% (w/v) PFA in PBS. The cells were then permeabilized with 1% NP-40 (Nonidet P40) in PBS and blocked with 0.5% fish-skin gelatin in PBS. The FLAG-tagged proteins were then localized with a mouse anti-FLAG antibody (M2, Sigma–Aldrich) and the ribosomes were localized with a rabbit anti-L26 protein antibody (Sigma–Aldrich). Secondary antibodies were Alexa Fluor®-488-conjugated goat anti-(mouse IgG) and Alexa Fluor®-594-conjugated goat anti-(rabbit IgG) (Molecular Probes) respectively. The cells were imaged on either a Zeiss LSM510 confocal microscope using an alpha Plan-Fluar 100× objective (numerical aperture 1.45) or a Leica sp2 confocal microscope using a HCX PL APO 63× objective (numerical aperture 1.40).

Crystallization and structure determination

*Lpp*GT was spin-concentrated to 26 mg/ml and chemically methylated following the protocol described by Walter et al. [17]. Crystals were grown by sitting-drop experiments at 20°C, mixing 1 μl of protein, containing 10 mM UDP-glucose and 2 mM $MnCl_2$, with an equal volume of a reservoir solution {0.1 M Hepes, pH 7.5, 20% (w/v) PEG [poly(ethylene glycol)] 3000 and 0.2 M NaCl}. Under these conditions, crystals appeared within 7–14 days. They were cryoprotected with 0.1 M Hepes, pH 7.5, 20% (v/v) glycerol, 20% (w/v) PEG 3000 and 0.2 M NaCl, and flash-cooled prior to data collection at 100 K.

Following a similar protocol, *Lpl*GT was spin-concentrated to 18 mg/ml and co-crystallized with 10 mM UDP-glucose and 2 mM $MnCl_2$. Crystals were grown in 0.1 M acetamido iminodiacetic acid, pH 6.5, 12% PEG 6000 and 0.1 M $MgCl_2$. MPD (2-methyl-2,4-pentanediol) at 20% (v/v) in mother liquor was used as a cryoprotectant.

A mercury-chloride-derivative of *Lpl*GT was generated by soaking experiments in mother liquor, supplemented with 100 mM $HgCl_2$, for 3–20 min prior to data collection. Data for the native crystals and the heavy-atom-derivative were collected at beamlines ID23-1/BM14 (European Synchrotron Radiation Facility, Grenoble, France). All data were processed and scaled using the HKL suite [18] and CCP4 software [19]; relevant statistics are given in Table 1.

By using SIRAS (single isomorphous replacement with anomalous scattering) methodology, with data from a crystal soaked with $HgCl_2$, as well as a data set on a crystal of the *Lpl*GT co-crystallized with UDP-glucose (Table 1), macromolecular phasing with SHELX C/D/E (using the HKL2MAP graphical user interface [20]) identified six sites, yielding phases with a figure of merit of 0.72 to 2.1 Å (1 Å = 0.1 nm). An initial model for *Lpl*GT was built using ARP/wARP software [21] (building 370 residues of the single protein monomer in the asymmetric unit) and improved through cycles of manual model building in Coot [22] and refinement with REFMAC5 [23]. Molecular replacement with this structure was used to generate phases and a starting model for *Lpp*GT, which was refined using similar procedures. Topologies for UDP-glucose, UDP and glucose ligands were generated with PRODRG [24]. The final models were validated with PROCHECK [25] and WHATCHECK [26]; model statistics are given in Table 1.

Bacterial strains

The *L. pneumophila* strains used in this study were *L. pneumophila* JR32, a streptomycin-resistant, restriction-negative mutant of *L. pneumophila Philadelphia*-1, which is a wild-type strain in terms of intracellular growth [27], and GS3011, an *icm*T-deletion mutant [28].

Construction of CyaA (adenylate cyclase toxin) fusions

All genes examined were amplified by PCR using a pair of primers (Supplementary Table S1) containing suitable restriction sites at the 5′ end. The PCR products were subsequently digested with the relevant enzymes and cloned into the pMMB-cyaA–C or pMMB-cyaA–N vectors [29], to generate the plasmids listed in Supplementary Table S2 (available at http://www.BiochemJ.org/bj/426/bj4260281add.htm), all the inserts were sequenced to verify that no mutations were incorporated during the PCR.

Analyses performed with host cells

Intracellular growth assays in *Acanthamoeba castellanii* and in human promyelocytic leukaemia HL-60-derived macrophages were performed essentially as described previously [30]. The CyaA translocation assay was performed as described previously [31].

RESULTS AND DISCUSSION

*Lp*GT adopts the GT-A fold with a flexible donor-binding loop

*Lpp*GT was cloned and expressed in *E. coli* as a GST (glutathione transferase) fusion protein and purified by affinity and gelfiltration chromatography. *Lpp*GT initially failed to produce diffraction quality crystals. Chemical methylation of solvent-exposed lysine residues led to a protein sample that produced a single, well-diffracting crystal (Table 1) for which the phase problem could not be solved. Our attention then shifted to the orthologous protein from *L. pneumophila* strain *Lens, Lpl*GT, which was cloned, expressed and purified using a similar strategy, readily producing well-diffracting crystals. The structure of *Lpl*GT bound to UDP-glucose was solved using a SIRAS experiment with a mercury derivative (Table 1 and Figure 1). The phase problem of the *Lpp*GT diffraction data (later found to include ordered UDP and glucose in the active site) was then solved by molecular replacement (Figure 1). Both structures were refined to high resolution, yielding final models with good *R*-factors (Table 1).

The structures of *Lpp*GT/*Lpl*GT reveal three domains: a completely α-helical (α1–α7) N-terminal domain, a central domain, containing the double Rossmann fold-like signature typical of the GT-A fold (α8–α15/β1–β10) with a central β-sheet surrounded by α-helices on both sides, and a third domain, which we term the ‘protrusion domain’. The protrusion domain is an unusual α-helical protrusion from the GT-A fold, consisting mainly of α-

helices (α16–α30) and two small β-strands (β11–β12). The well-defined density for Mg^{2+}-UDP-glucose (*Lpl*GT) and Mn^{2+}–UDP-glucose (*Lpp*GT), observed in the donor site, was almost completely formed by the central subdomain and a long C-terminal loop coming from the third domain (Figure 1A, see also Figure 4).

A comparison between the *Lpp*GT and *Lpl*GT structures revealed some conformational change within the N-terminal domains [RMSD (root mean square deviation) of 0.4 Å for 82 aligned Cα atoms] and differences in order/disorder of a number of regions, such as in a loop in the α-helical protrusion domain and in the C-terminal loop (residues 509–520; Figure 1A and see Supplementary Figure S1 available at http://www.BiochemJ.org/bj/426/bj4260281add.htm). Although these conformational changes could have resulted from differences in crystal packing (Table 1) or bound ligands (*Lpl*GT with Mg^{2+}–UDP-glucose and *Lpp*GT with Mn^{2+}–UDP-glucose), there have been many examples of metal- or donor-induced conformational changes of loops/regions in glycosyltransferases that contribute to formation of the acceptor-binding site [32]. In the *Lp*GT structures, the flexible C-terminal loop was particularly well positioned to create the acceptor-binding site upon binding to the metal and UDP-glucose (Figure 1A).

LpGT is structurally homologous to *C. difficile* TcdB and two other *Legionella* glucosyltransferases

Surprisingly, analysis of the *Lp*GT structures with the DALI server [33] revealed structural homology to *C. difficile* TcdB (PDB codes 2BVL and 2BVM [34]), *Clostridium novyi* α-toxin (PDB code 2VK9 [35]) and *Clostridium sordellii* lethal toxin (PDB codes 2VKD and 2VKH [35]). Whereas structure-based sequence alignments showed very low identities (14–18% with 185–199 aligned residues; Figure 2), the structural GT-A cores superimposed well (RMSDs of 2.5–3.2 Å, Figures 1A–1C). For example, TcdB is formed by the typical two abutting Rossmann-like folds, which creates the sugar-donor-binding site (Figure 1), and superimposed well with some secondary structures, such as β3–β10, α8, α11–α13 and α15 from *Lp*GT (Figures 1B and 1C).

A recent study has identified two further putative *Legionella* glucosyltransferases, Lgt2 (also known as LegC8) and Lgt3 (also known as LegC5), which are 72 kDa and 100 kDa proteins respectively, with additional multiple coiled-coil domains [36]. Although sequence alignments show a low level of overall sequence identity (18–28%; Figure 2), the crystal structures reveal several regions of high conservation, not only including the UDP-glucose-binding site and putative catalytic residues but also a putative acceptor-binding groove (Figure 1D). Furthermore, it was also shown that these three *Legionella* enzymes all possess glycosyl-transferase activity against hEF1A and kill eukaryotic cells [36].

Identification of the putative hEF1A-docking site

Structural analysis of the known hEF1A glucosylation site at Ser^{53}, using the *Sc*EF1A structure (*Saccharomyces cerevisiae* E1FA; PDB code 2B7B [37]), reveals this to be located at the tip of a loop between two helices extending approx. 20 Å from the surface of the protein. Ser^{53} is flanked by two lysine residues, which are conserved between hEF1A and *Sc*EF1A, giving the tip of this loop on overall positive charge (Figure 3). Interestingly, electrostatic analysis of the conserved putative acceptor-binding site in *Lp*GT reveals an overall negative charge (Figures 1D and 3), suggesting electrostatic complementarity between *Lp*GT and the elongation factor glucosylation site. Using the constraints of the location of the UDP-glucose anomeric carbon, the Ser^{53} glucosylation site and the overall shape of the *Lp*GT/*Sc*EF1A proteins, it is possible to approximately position *Sc*EF1A in the *Lp*GT acceptor site, with qualitative shape-complementarity (Figure 3). To test this model of interaction, we targeted a key exposed aromatic residue, Tyr^{454}, which lines the putative

Europe PMC Funders Author Manuscripts

acceptor-binding site (Figure 3), by mutagenesis. Mutation of this residue to alanine led to a reduction in the activity towards hEF1A in HEK-293 lysates, whereas it did not significantly affect UDP-glucose binding (see Figure 5A and Table 2), suggesting an approximate identification of an EF1A-docking site on *Lp*GT.

LppGT/LplGT binds UDP-glucose through loops from the central and protrusion domain

The two crystal structures described in the present paper reflect two different states during catalysis (Figure 4). The structure of *Lpl*GT was solved in complex with UDP-glucose and Mg^{2+}, resembling the substrate-binding mode. The *Lpp*GT structure was solved in complex with UDP, glucose and Mn^{2+}, resembling a product complex (Figure 4). In both structures, the nucleotides occupied the same positions and adopted the same conformations, with a shift in position observed for the glucose (maximum atomic shift of 1.6 Å). The nucleotide was located between three loops: α12–α13, α4–α8 and the C-terminal loop (which was disordered in the *Lpl*GT structure, where only residues 518–523 were visible; Figures 1A and 4). The uracil ring was sandwiched between Trp^{139} (β4–α8 loop) and Pro^{225} (located at the beginning of α13) by hydrophobic stacking interactions (Figure 4). With the exception of these two hydrophobic contacts, the majority of the interactions occurred through hydrogen bonds with backbone residues from Ile^{138}, Trp^{139}, Phe^{140}, Ile^{142}, Ile^{247} and Ser^{519} (Figure 4). Moreover, the phosphate group oxygen atoms were recognized by hydrogen bonds with the Ser^{519} and Trp^{520} side chains in the *Lpl*GT structure and, as a result of the shift in position of the glucose, Asn^{499}, Asn^{514} and Trp^{520} side chains and the Leu^{518} backbone residue in the *Lpp*GT structure (Figure 2). Although Ser^{519} has a hydrogen bond with the UDP α-phosphate, mutation of this residue affected neither UDP-glucose binding nor activity (Figure 4 and Table 2). A structural comparison with TcdB showed that two conserved residues, Trp^{102} and Trp^{520} in TcdB (Figure 4), are involved in binding to uridine and phosphate groups, and are present in all GT44 *Clostridium* and GT88 *Legionella* enzymes, and they hence present a common sequence signature in these two large families of enzymes. Mutagenesis has shown that the Trp^{102} and Trp^{520} residues of TcdB are important for UDP-glucose binding and catalysis [38,39].

The DxD motif is essential for catalysis but not for donor binding

The active-site metals of GT-A-fold glycosyltransferases are known to have two roles: to induce a conformational change in a flexible loop and to stabilize a transition state during catalysis, with the help of two key aspartic acids in an Asp-Xaa-Asp or DxD motif [32,40,41]. The phosphate group oxygen atoms, Asp^{248} of the DxD motif and two ordered water molecules appear to pentagonally co-ordinate the metal (Mg^{2+}) in the *Lpl*GT structure, whereas the *Lpp*GT reveals a hexagonally co-ordinated Mn^{2+}, using an additional water molecule and with Asp^{246} instead of Asp^{248} (Figure 4); this is accompanied by a shift of 1.8 Å in the position of the metal. The importance of the DxD motif in *Lp*GT has been investigated previously using the D246N single or D246N/D248N double mutants, which result in a decrease in glucosyltransfer activity against hEF1A [7]. We investigated the role of these residues further to dissect the effects on donor binding and activity. The D248A mutant showed no significant reduction of overall activity, but binding of UDP-glucose was an order of magnitude weaker as measured by tryptophan fluorescence (Figure 5A and Table 2), in agreement with the donor-binding role of the aspartic acid residues in the DxD motif, as proposed previously [42,43]. However, the D246A mutant showed a significant reduction in activity compared with the *Lpp*GT wild-type enzyme, with only a moderate reduction in donor binding (Figure 5A and Table 2). Strikingly, the D246A/D248A double mutant had no detectable activity and reduced binding of UDP-glucose by an order of magnitude (Figure 5A and Table 2). Thus the aspartic acid residues in the DxD motif may have roles in stabilization of the transition state and activity, as proposed previously by Qasba et al. [32], in addition to being important, although not essential, for binding of UDP-glucose [42-44].

In the substrate complex, glucose is hydrogen-bonded to Asp^{230}, Arg^{233} and Asp^{246}, whereas in the product-binding mode structure Asn^{293} has this role instead of Asp^{246}. These changes in hydrogen bonding and the position of the DxD motif may reflect the shift in ligand position and the identity of the metal (Figure 4). Interestingly, two of the glucose-interacting residues (Asp^{230} and Arg^{233}) are conserved in TcdB (Asp^{270} and Arg^{273} respectively; Figure 4). Mutation of these residues in TcdB had significant effects on binding to UDP-glucose and activity [39].

The *Lp*GT active site structure confirms a retaining mechanism with two catalytic asparagine residues

TcdB belongs to a large family of GT-A glycosyltransferases with retaining character [45]. Among this family, the better characterized enzymes include the *Neisseria meningitidis* galactosyltransferase, LgtC [42,46-48], the bovine α-1,3-galactosyltransferase, 3GalT [49], the two enzymes responsible for the formation of blood type A and B, GTA (α-1,3-N-acetylgalactosaminyltransferase) and GTB (α-1,3-galactosyltransferase) [50-52] respectively, ppGalNAcTs (polypeptide N-α-acetylgalactosaminyltransferases) [53-55] and MGS (mannosylglycerate synthase) [56]. For these retaining enzymes, a glutamine or glutamic acid residue has been proposed as the catalytic nucleophile involved in a $D_N{*}A_{Nss}$ ion-pair mechanism [45]. Comparison of *Lp*GT, TcdB and other retaining glycosyltransferase active sites suggests that *Lp*GT may follow a retaining mechanism (Figure 4), in agreement with recent work that has established a retaining mechanism for this enzyme by NMR spectroscopy [12]. The structures reveal not only conservation of the DxD motif and glucose-binding residues, but also a key asparagine residue (Asn^{293}), positioned approx. 4 Å away from the anomeric carbon, in a similar manner to Gln^{189} in LgtC and Asn^{384} in TcdB, which are proposed to be involved in a back-side nucleophilic push [42,45]. We mutated all *Lp*GT residues close to the anomeric carbon, including Asn^{293} and Asn^{499}, as well as Glu^{445} and Glu^{446}, two residues positioned such that they could possibly act as a catalytic base if *Lp*GT employed an inverting mechanism (Figure 4). As expected, none of these residues affected binding of UDP-glucose (Table 2), a result which also confirmed that these mutant proteins were properly folded. Furthermore, mutation of the two glutamate residues did not affect activity of *Lp*GT towards hE1FA in cell lysates (Figure 5A). Strikingly, however, mutation of either Asn^{293} or Asn^{499} resulted in mutant enzymes without any detectable glucosyltransfer activity (Figure 5A). Thus these mutations confirm that *Lp*GT follows a retaining catalytic mechanism as proposed for *C. difficile* toxin and other glycosyltransferases [42,45-48]. Given the position of the two asparagine residues, Asn^{293} could act as the weak nucleophile involved in pushing the anomeric carbon during the Sn_i (substitution nucleophilic internal)-like mechanism (through a $D_N{*}A_{Nss}$ ion-pair) and Asn^{499} may play an essential role in stabilizing the transition state and the leaving group.

Inactive LpGT mutants are impaired in induction of HeLa cell apoptosis

Although it is known that the toxicity of *Lp*GT stems from its glucosylation of hEF1A, the precise mechanism of cell death is as yet unclear. Immunofluorescence microscopy analysis of HeLa cells microinjected with wild-type *Lpp*GT suggested that the cells die with typical hallmarks of apoptosis, such as clumped DNA in the nuclei, plasma membrane blebbing and dead cells in phagosomes of adjoining cells (Figure 5B and Supplementary Figure S2 available at http://www.BiochemJ.org/bj/426/bj4260281add.htm). More studies will be required to address how these enzymes, in addition to disruption of ribosome translation, induce apoptosis in mammalian cells.

We repeated the microinjection experiments using the *Lpp*GT mutants generated as part of the present study. Although all the mutants and wild-type *Lpp*GT showed some detectable

levels of cell death within 48 h, as reported previously [7], all the mutants, with the exception of the D246A and D248A single mutants (from the DxD motif), showed a significant reduction in cell death compared with the wild type (Figure 5B and Table 2). The fact that the catalytically inactive mutants protected against cell death but not growth suggests that the toxicity of *Lpp*GT does not entirely depend on its glucosyltransferase activity. It is possible that the inactive mutants are still able to disrupt protein–protein complexes or deplete hEF1A levels.

LppGT, Lgt2 and Lgt3 are exported through the Icm/Dot machinery

Although *Lpp*GT, Lgt2 and Lgt3 have been shown to kill mammalian cells in electroporation experiments [7,36], and we also see cell death in microinjection studies (as described above), it is as yet unclear how these enzymes are exported from *Legionella* into the macrophages. It is worth noting that a range of known *Legionella* virulence factors are substrates for the Icm/Dot system used by the bacterium to secrete virulence factors into the macrophage cytosol [10,57,58]. We tested whether *Lpp*GT, LegC5 and LegC8 were substrates for the Icm/Dot system by N-terminally fusing these enzymes to inactive CyaA, and stably expressing the proteins in *L. pneumophila* strain JR32. These stable transfectants were used to infect HL-60-derived macrophages, and cAMP levels were determined to follow translocation [30]. In agreement with a previous study [59,60], Lgt3 was translocated into the macrophage and similar results were obtained for Lgt2 (Figure 5C). Surprisingly, however, no significant cAMP levels were detected for *Lpp*GT (results not shown for an N-terminal fusion of *Lpp*GT with CyaA). The majority of the *L. pneumophila* Icm/Dot substrates are known to contain a C-terminal signal sequence [61]. Interestingly, the only crystal structure of a type IV effector, RalF [62], shows a C-terminal disordered region within the last 20 residues as the signal sequence [62,63], and secondary structure predictions suggest the Lgt3 and Lgt2 C-termini contain a similar number of disordered amino acids. However, the *Lpp*GT structure shows that the C-terminus is well-ordered and, indeed, forms part of the active site (Figure 1A). Thus we decided to repeat the secretion experiment with a C-terminal fusion of *Lpp*GT with CyaA. Strikingly, this led to translocation into macrophages (Figure 5C), suggesting that, unusually, *Lp*GT contains its type IV signal sequence at the N-terminus (Figures 1A and 5C). The N-terminus of *Lpp*GT is α-helical with only the first ten residues being completely disordered. It is not clear whether these residues are necessary and sufficient as a type IV secretion signal or whether a structural motif may be required for recognition by the Icm/Dot machinery. With the exception of *Lp*GT, only two other previous studies report cases of effector proteins carrying N-terminal type IV signal peptides [60,64]. Taken together, these results are consistent with a model whereby *Lpp*GT, Lgt2 and Lgt3 are virulence factors; they are ejected by *L. pneumophila* into the macrophage and contribute to cell death through inhibition of protein synthesis.

Considering the differences in sequence and length between *Lp*GT, Lgt2 and Lgt3, it is possible that these enzymes show differences in localization in mammalian cells. To study this, we expressed C-terminally FLAG-tagged versions of these enzymes (which retain full activity; results not shown) in *E. coli* and microinjected these into HeLa cells. Despite the significant differences in sequence and length (Figure 2), all three were diffusely distributed throughout the cell, showing some co-localization with the ribosomal L26 protein, in agreement with hE1FA being one of the substrates of these enzymes (localization of *Lpp*GT shown in Figure 5D; results not shown for Lgt2 and Lgt3).

Conclusions

Legionella is an accidental intracellular infectious bacterium. During the life cycle in the host macrophage, the bacterium needs to tightly control host cell processes to allow optimal

replication without (initially) killing the host. At the end of the replication stage, apoptosis is induced and bacteria are released. Numerous effectors have been described, and some cases of redundancy have been reported [58,65,66]. In the present study we have investigated a family of redundant glucosyltransferases, which kill mammalian host macrophages by apoptosis through post-translational modification of hEF1A and other, as yet unknown, mechanisms which are independent of their catalytic activity (as suggested by our microinjection studies with inactive mutants). Our data suggest redundancy in localization and activity and reveals the *Lp*GT, Lgt2 and Lgt3 are all Icm/Dot effectors, consistent with the notion that they are virulence factors.

It is not clear why *L. pneumophila* would inject these three proteins with similar activities and localization patterns into the host cell. Studies carried out by Belyi et al. [36] show that *Lp*GT and Lgt2 are produced at the beginning of the stationary phase of its growth curve, whereas Lgt3 is only produced at the early stage of the growth curve. Thus it is possible that *Legionella* only makes these proteins in the slowly replicating and non-dividing stages, either at the beginning or at the end of host infection. There are many other examples of *Legionella* secreting redundant virulence factors; DrrA and SidM [58], which are a GEF and GDF (GDI displacement factor) respectively, LidA [65], which binds to Rab1-GTP and LepB [66], which is a GAP (GTPase-activating protein), are all involved in the human Rab1 cycle. Similarly, *Lpp*GT, Lgt2 and Lgt3 may form a redundant mammalian killer toxin family, which may be relevant to start new infections and produce host death by apoptosis in order to infect new cells. In order to address how important these enzymes are in the *Legionella* infection cycle, studies with single, double and triple knockouts should be performed.

Our structural studies show that *Lp*GT is a metal-dependent enzyme, which possesses a GT-A fold. This structure supports the notion that Lgt2 and Lgt3 are also active glycosyltransferases, possessing conserved UDP-glucose and acceptor-binding sites. Structural and mutation analyses suggest that a negatively charged binding groove in *Lp*GT may recognize a positively charged loop in EF1A which carries the acceptor serine residue. Mutagenesis studies on several amino acids in the active site suggest that *Lp*GT may employ a retaining mechanism involving two catalytic residues: Asn^{293} acting as the weak nucleophile, and Asn^{499} stabilizing the transition state and the UDP leaving-group. It appears that the DxD motif is important for catalysis, yet not essential for donor binding.

In conclusion, *Lp*GT, Lgt2 and Lgt3 are a redundant set of virulence factors forming a glucosyltransferase family with a conserved putative EF1A-binding site and acting via a retaining mechanism. The present study will form the basis for future studies towards the protein substrate specificity of these enzymes and the development of chemical biological probes for further cell biological studies of these virulence factors.

Supplementary Material

Refer to Web version on PubMed Central for supplementary material.

Acknowledgments

We thank the European Synchrotron Radiation Facility, Grenoble, France, for beamtime.

FUNDING

This work was supported by a Wellcome Trust Senior Research Fellowship and a Medical Research Council Programme grant (to Daan van Aalten).

Abbreviations used

CyaA	adenylate cyclase toxin
CAZY	carbohydrate-active enzyme
DAPI	4′,6-diamidino-2-phenylindole
DTT	dithiothreitol
EF1A	elongation factor 1A
GEF	guanine nucleotide exchange factor
GST	glutathione transferase
HEK	human embryonic kidney
Icm/Dot	intracellular multiplication/defect in organelle trafficking
Lgt2	*L. pneumophila* glucosyltransferase 2
Lgt3	*L. pneumophila* glucosyltransferase 3
LgtC	*N. meningitidis* galactosyltransferase
***Lp*GT**	*L. pneumophila* glucosyltransferase
***Lpl*GT**	*Lp*GT from strain *Lens*
***Lpp*GT**	*Lp*GT from strain *Philadelphia*-1
PEG	poly(ethylene glycol)
PFA	paraformaldehyde
RMSD	root mean square deviation
SIRAS	single isomorphous replacement with anomalous scattering
TcdB	*C. difficile* toxin B

REFERENCES

1. Coutinho, PM.; Henrissat, B. Carbohydrate-active enzymes: an integrated database approach. In: Gilbert, HJ.; Davies, G.; Henrissat, B.; Svensson, B., editors. Recent Advances in Carbohydrate Bioengineering. The Royal Society of Chemistry; Cambridge: 1999. p. 3-12.
2. Just I, Selzer J, Wilm M, von Eichel-Streiber C, Mann M, Aktories K. Glucosylation of Rho proteins by *Clostridium difficile* toxin B. Nature. 1995; 375:500–503. [PubMed: 7777059]
3. Schirmer J, Aktories K. Large clostridial cytotoxins: cellular biology of Rho/Ras-glucosylating toxins. Biochim. Biophys. Acta. 2004; 1673:66–74. [PubMed: 15238250]
4. Lyerly, D.; Wilkins, TD. Clostridium difficile. Raven Press; New York: 1995.
5. Jank T, Giesemann T, Aktories K. Rho-glucosylating *Clostridium difficile* toxins A and B: new insights into structure and function. Glycobiology. 2007; 17:15R–22R.
6. Belyi I, Popoff MR, Cianciotto NP. Purification and characterization of a UDP-glucosyltransferase produced by *Legionella pneumophila*. Infect. Immun. 2003; 71:181–186. [PubMed: 12496164]
7. Belyi Y, Niggeweg R, Opitz B, Vogelsgesang M, Hippenstiel S, Wilm M, Aktories K. *Legionella pneumophila* glucosyltransferase inhibits host elongation factor 1A. Proc. Natl. Acad. Sci. U.S.A. 2006; 103:16953–16958. [PubMed: 17068130]
8. Albert-Weissenberger C, Cazalet C, Buchrieser C. *Legionella pneumophila*: a human pathogen that co-evolved with fresh water protozoa. Cell. Mol. Life Sci. 2007; 64:432–448. [PubMed: 17192810]
9. Kumpers P, Tiede A, Kirschner P, Girke J, Ganser A, Peest D. Legionnaires' disease in immunocompromised patients: a case report of *Legionella longbeachae* pneumonia and review of the literature. J. Med. Microbiol. 2008; 57:384–387. [PubMed: 18287305]

10. Ninio S, Roy CR. Effector proteins translocated by *Legionella pneumophila*: strength in numbers. Trends Microbiol. 2007; 15:372–380. [PubMed: 17632005]
11. Shin S, Roy CR. Host cell processes that influence the intracellular survival of *Legionella pneumophila*. Cell. Microbiol. 2008; 10:1209–1220. [PubMed: 18363881]
12. Belyi Y, Stahl M, Sovkova I, Kaden P, Luy B, Aktories K. Region of elongation factor 1A1 involved in substrate recognition by *Legionella pneumophila* glucosyltransferase Lgt1: identification of Lgt1 as a retaining glucosyltransferase. J. Biol. Chem. 2009; 284:20167–20174. [PubMed: 19478083]
13. Bradford MM. A rapid and sensitive method for the quantitation of microgram quantities of protein utilizing the principle of protein-dye binding. Anal. Biochem. 1976; 72:248–254. [PubMed: 942051]
14. Neumann B, Held M, Liebel U, Erfle H, Rogers P, Pepperkok R, Ellenberg J. High-throughput RNAi screening by time-lapse imaging of live human cells. Nat. Methods. 2006; 3:385–390. [PubMed: 16628209]
15. Izant JG, Weatherbee JA, McIntosh JR. A microtubule-associated protein antigen unique to mitotic spindle microtubules in PtK1 cells. J. Cell. Biol. 1983; 96:424–434. [PubMed: 6339516]
16. Prescott AR, Dowrick PG, Warn RM. Stable and slow-turning-over microtubules characterize the processes of motile epithelial cells treated with scatter factor. J. Cell Sci. 1992; 102:103–112. [PubMed: 1386851]
17. Walter TS, Meier C, Assenberg R, Au KF, Ren J, Verma A, Nettleship JE, Owens RJ, Stuart DI, Grimes JM. Lysine methylation as a routine rescue strategy for protein crystallization. Structure. 2006; 14:1617–1622. [PubMed: 17098187]
18. Otwinowski Z, Minor W. Processing of X-ray diffraction data collected in oscillation mode. Methods Enzymol. 1997; 276:307–326.
19. Collaborative Computational Project. The CCP4 Suite: Programs for Protein Crystallography. Acta Crystallogr. D Biol. Crystallogr. 1994; 50:760–763. [PubMed: 15299374]
20. Pape D, Seil R, Kohn D, Schneider G. Imaging of early stages of osteonecrosis of the knee. Orthop. Clin. North Am. 2004; 35:293–303. viii. [PubMed: 15271537]
21. Perrakis A, Morris R, Lamzin VS. Automated protein model building combined with iterative structure refinement. Nat. Struct. Biol. 1999; 6:458–463. [PubMed: 10331874]
22. Emsley P, Cowtan K. Coot: model-building tools for molecular graphics. Acta Crystallogr. D Biol. Crystallogr. 2004; 60:2126–2132. [PubMed: 15572765]
23. Murshudov GN, Vagin AA, Dodson EJ. Refinement of macromolecular structures by the maximum-likelihood method. Acta Crystallogr. D Biol. Crystallogr. 1997; 53:240–255. [PubMed: 15299926]
24. Schuttelkopf AW, van Aalten DM. PRODRG: a tool for high-throughput crystallography of protein-ligand complexes. Acta Crystallogr. D Biol. Crystallogr. 2004; 60:1355–1363. [PubMed: 15272157]
25. Laskowski RA, Moss DS, Thornton JM. Main-chain bond lengths and bond angles in protein structures. J. Mol. Biol. 1993; 231:1049–1067. [PubMed: 8515464]
26. Hooft RW, Vriend G, Sander C, Abola EE. Errors in protein structures. Nature. 1996; 381:272. [PubMed: 8692262]
27. Sadosky AB, Wiater LA, Shuman HA. Identification of *Legionella pneumophila* genes required for growth within and killing of human macrophages. Infect. Immun. 1993; 61:5361–5373. [PubMed: 8225610]
28. Zusman T, Yerushalmi G, Segal G. Functional similarities between the icm/dot pathogenesis systems of *Coxiella burnetii* and *Legionella pneumophila*. Infect. Immun. 2003; 71:3714–3723. [PubMed: 12819052]
29. Zusman T, Aloni G, Halperin E, Kotzer H, Degtyar E, Feldman M, Segal G. The response regulator PmrA is a major regulator of the icm/dot type IV secretion system in *Legionella pneumophila* and *Coxiella burnetii*. Mol. Microbiol. 2007; 63:1508–1523. [PubMed: 17302824]
30. Segal G, Shuman HA. *Legionella pneumophila* utilizes the same genes to multiply within *Acanthamoeba castellanii* and human macrophages. Infect. Immun. 1999; 67:2117–2124. [PubMed: 10225863]

31. Altman E, Segal G. The response regulator CpxR directly regulates expression of several *Legionella pneumophila* icm/dot components as well as new translocated substrates. J. Bacteriol. 2008; 190:1985–1996. [PubMed: 18192394]
32. Qasba PK, Ramakrishnan B, Boeggeman E. Substrate-induced conformational changes in glycosyltransferases. Trends Biochem. Sci. 2005; 30:53–62. [PubMed: 15653326]
33. Holm L, Sander C. Dali: a network tool for protein structure comparison. Trends Biochem. Sci. 1995; 20:478–480. [PubMed: 8578593]
34. Reinert DJ, Jank T, Aktories K, Schulz GE. Structural basis for the function of *Clostridium difficile* toxin B. J. Mol. Biol. 2005; 351:973–981. [PubMed: 16054646]
35. Ziegler MO, Jank T, Aktories K, Schulz GE. Conformational changes and reaction of clostridial glycosylating toxins. J. Mol. Biol. 2008; 377:1346–1356. [PubMed: 18325534]
36. Belyi Y, Tabakova I, Stahl M, Aktories K. Lgt: a family of cytotoxic glucosyltransferases produced by *Legionella pneumophila*. J. Bacteriol. 2008; 190:3026–3035. [PubMed: 18281405]
37. Andersen GR, Pedersen L, Valente L, Chatterjee I, Kinzy TG, Kjeldgaard M, Nyborg J. Structural basis for nucleotide exchange and competition with tRNA in the yeast elongation factor complex eEF1A:eEF1Balpha. Mol. Cell. 2000; 6:1261–1266. [PubMed: 11106763]
38. Busch C, Hofmann F, Gerhard R, Aktories K. Involvement of a conserved tryptophan residue in the UDP-glucose binding of large clostridial cytotoxin glycosyltransferases. J. Biol. Chem. 2000; 275:13228–13234. [PubMed: 10788427]
39. Jank T, Giesemann T, Aktories K. *Clostridium difficile* glucosyltransferase toxin B: essential amino acids for substrate binding. J. Biol. Chem. 2007; 282:35222–35231. [PubMed: 17901056]
40. Ramakrishnan B, Qasba PK. Crystal structure of lactose synthase reveals a large conformational change in its catalytic component, the β-1,4-galactosyltransferase-I. J. Mol. Biol. 2001; 310:205–218. [PubMed: 11419947]
41. Charnock SJ, Davies GJ. Structure of the nucleotide-diphospho-sugar transferase, SpsA from *Bacillus subtilis*, in native and nucleotide-complexed forms. Biochemistry. 1999; 38:6380–6385. [PubMed: 10350455]
42. Persson K, Ly HD, Dieckelmann M, Wakarchuk WW, Withers SG, Strynadka NC. Crystal structure of the retaining galactosyltransferase LgtC from *Neisseria meningitidis* in complex with donor and acceptor sugar analogs. Nat. Struct. Biol. 2001; 8:166–175. [PubMed: 11175908]
43. Busch C, Hofmann F, Selzer J, Munro S, Jeckel D, Aktories K. A common motif of eukaryotic glycosyltransferases is essential for the enzyme activity of large clostridial cytotoxins. J. Biol. Chem. 1998; 273:19566–19572. [PubMed: 9677381]
44. Zhang Y, Malinovskii VA, Fiedler TJ, Brew K. Role of a conserved acidic cluster in bovine β-1,4 galactosyltransferase-1 probed by mutagenesis of a bacterially expressed recombinant enzyme. Glycobiology. 1999; 9:815–822. [PubMed: 10406847]
45. Lairson LL, Henrissat B, Davies GJ, Withers SG. Glycosyltransferases: structures, functions, and mechanisms. Annu. Rev. Biochem. 2008; 77:521–555. [PubMed: 18518825]
46. Lairson LL, Chiu CP, Ly HD, He S, Wakarchuk WW, Strynadka NC, Withers SG. Intermediate trapping on a mutant retaining α-galactosyltransferase identifies an unexpected aspartate residue. J. Biol. Chem. 2004; 279:28339–28344. [PubMed: 15075344]
47. Zhang Y, Swaminathan GJ, Deshpande A, Boix E, Natesh R, Xie Z, Acharya KR, Brew K. Roles of individual enzyme–substrate interactions by α-1,3-galactosyltransferase in catalysis and specificity. Biochemistry. 2003; 42:13512–13521. [PubMed: 14621997]
48. Jamaluddin H, Tumbale P, Withers SG, Acharya KR, Brew K. Conformational changes induced by binding UDP-2F-galactose to α-1,3 galactosyltransferase: implications for catalysis. J. Mol. Biol. 2007; 369:1270–1281. [PubMed: 17493636]
49. Gastinel LN, Bignon C, Misra AK, Hindsgaul O, Shaper JH, Joziasse DH. Bovine α-1,3-galactosyltransferase catalytic domain structure and its relationship with ABO histo-blood group and glycosphingolipid glycosyltransferases. EMBO J. 2001; 20:638–649. [PubMed: 11179209]
50. Yamamoto F, Clausen H, White T, Marken J, Hakomori S. Molecular genetic basis of the histo-blood group ABO system. Nature. 1990; 345:229–233. [PubMed: 2333095]

51. Patenaude SI, Seto NO, Borisova SN, Szpacenko A, Marcus SL, Palcic MM, Evans SV. The structural basis for specificity in human ABO(H) blood group biosynthesis. Nat. Struct. Biol. 2002; 9:685–690. [PubMed: 12198488]
52. Lee HJ, Barry CH, Borisova SN, Seto NO, Zheng RB, Blancher A, Evans SV, Palcic MM. Structural basis for the inactivity of human blood group O2 glycosyltransferase. J. Biol. Chem. 2005; 280:525–529. [PubMed: 15475562]
53. Fritz TA, Hurley JH, Trinh LB, Shiloach J, Tabak LA. The beginnings of mucin biosynthesis: the crystal structure of UDP-GalNAc:polypeptide α-N-acetylgalactosaminyltransferase-T1. Proc. Natl. Acad. Sci. U.S.A. 2004; 101:15307–15312. [PubMed: 15486088]
54. Kubota T, Shiba T, Sugioka S, Furukawa S, Sawaki H, Kato R, Wakatsuki S, Narimatsu H. Structural basis of carbohydrate transfer activity by human UDP-GalNAc: polypeptide α-N-acetylgalactosaminyltransferase (pp-GalNAc-T10). J. Mol. Biol. 2006; 359:708–727. [PubMed: 16650853]
55. Fritz TA, Raman J, Tabak LA. Dynamic association between the catalytic and lectin domains of human UDP-GalNAc:polypeptide α-N-acetylgalactosaminyltransferase-2. J. Biol. Chem. 2006; 281:8613–8619. [PubMed: 16434399]
56. Flint J, Taylor E, Yang M, Bolam DN, Tailford LE, Martinez-Fleites C, Dodson EJ, Davis BG, Gilbert HJ, Davies GJ. Structural dissection and high-throughput screening of mannosylglycerate synthase. Nat. Struct. Mol. Biol. 2005; 12:608–614. [PubMed: 15951819]
57. Shohdy N, Efe JA, Emr SD, Shuman HA. Pathogen effector protein screening in yeast identifies *Legionella* factors that interfere with membrane trafficking. Proc. Natl. Acad. Sci. U.S.A. 2005; 102:4866–4871. [PubMed: 15781869]
58. Murata T, Delprato A, Ingmundson A, Toomre DK, Lambright DG, Roy CR. The *Legionella pneumophila* effector protein DrrA is a Rab1 guanine nucleotide-exchange factor. Nat. Cell Biol. 2006; 8:971–977. [PubMed: 16906144]
59. De Buck E, Anne J, Lammertyn E. The role of protein secretion systems in the virulence of the intracellular pathogen *Legionella pneumophila*. Microbiology. 2007; 153:3948–3953. [PubMed: 18048909]
60. de Felipe KS, Pampou S, Jovanovic OS, Pericone CD, Ye SF, Kalachikov S, Shuman HA. Evidence for acquisition of *Legionella* type IV secretion substrates via interdomain horizontal gene transfer. J. Bacteriol. 2005; 187:7716–7726. [PubMed: 16267296]
61. Cambronne ED, Roy CR. The *Legionella pneumophila* IcmSW complex interacts with multiple Dot/Icm effectors to facilitate type IV translocation. PLoS Pathog. 2007; 3:e188. [PubMed: 18069892]
62. Nagai H, Cambronne ED, Kagan JC, Amor JC, Kahn RA, Roy CR. A C-terminal translocation signal required for Dot/Icm-dependent delivery of the *Legionella* RalF protein to host cells. Proc. Natl. Acad. Sci. U.S.A. 2005; 102:826–831. [PubMed: 15613486]
63. Nagai H, Kagan JC, Zhu X, Kahn RA, Roy CR. A bacterial guanine nucleotide exchange factor activates ARF on *Legionella* phagosomes. Science. 2002; 295:679–682. [PubMed: 11809974]
64. Chen J, Reyes M, Clarke M, Shuman HA. Host cell-dependent secretion and translocation of the LepA and LepB effectors of *Legionella pneumophila*. Cell Microbiol. 2007; 9:1660–1671. [PubMed: 17371403]
65. Machner MP, Isberg RR. Targeting of host Rab GTPase function by the intravacuolar pathogen *Legionella pneumophila*. Dev. Cell. 2006; 11:47–56. [PubMed: 16824952]
66. Ingmundson A, Delprato A, Lambright DG, Roy CR. *Legionella pneumophila* proteins that regulate Rab1 membrane cycling. Nature. 2007; 450:365–369. [PubMed: 17952054]

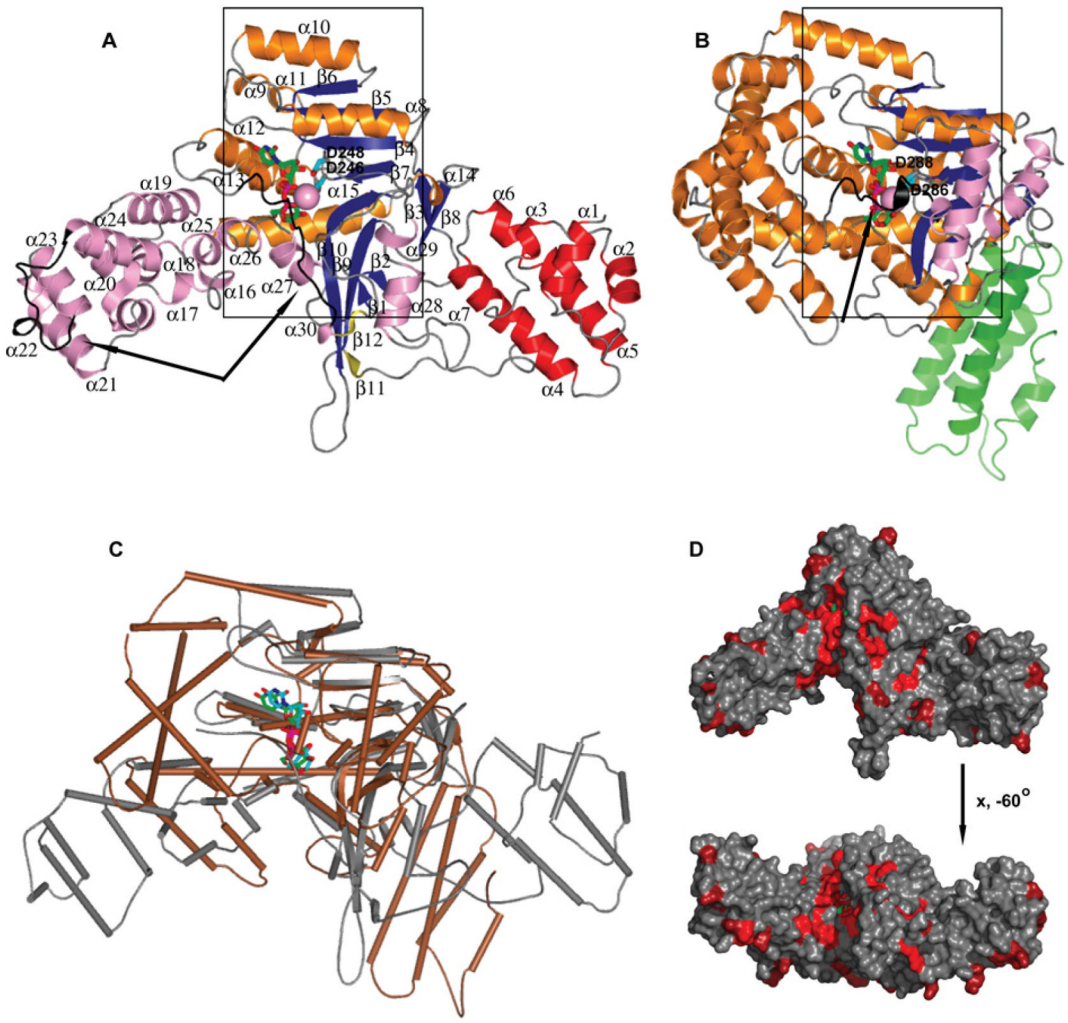

Figure 1. Structure of *Lp*GT

(**A**) Ribbon diagram of *Lpp*GT crystal structure in complex with UDP, glucose and manganese. (**B**) Comparison of *Lpp*GT crystal structure with TcdB (PDB codes 2BVL and 2BVM [34]). Secondary structures are represented in red and green for α-helixes of *Lpp*GT and toxin B N-terminal domain, brown and blue for α-helixes and β-strands in central domain of *Lpp*GT and toxin B, and pink and olive colour for α-helixes and β-strands of the C-terminal protrusion domain of *Lpp*GT and toxin B respectively. UDP and glucose are shown in green sticks and manganese as a pink sphere. The two aspartic acid residues (Asp^{246} and Asp^{248} in *Lpp*GT) are shown as cyan sticks. Arrows indicate flexible regions in both crystal structures. (**C**) Superposition of *Lpp*GT (grey) and TcdB (brown). UDP and glucose are shown in green and blue sticks in *Lpp*GT and TcdB respectively. (**D**) Surface representation of the *Lpp*GT enzyme, coloured by sequence conservation with Lgt2 and Lgt3 (from red, 100% identity, to grey, <50% identity).

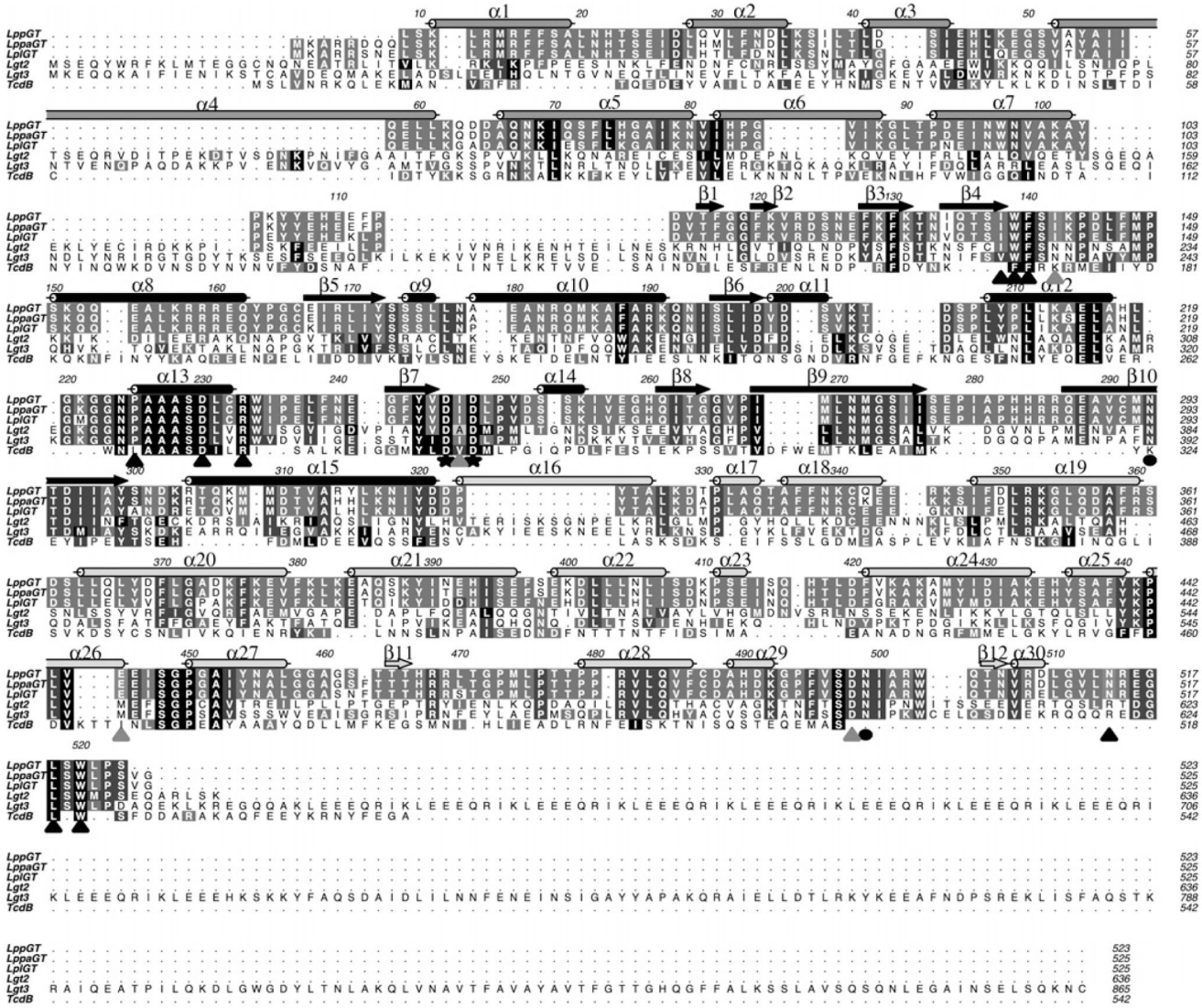

Figure 2. Multiple sequence alignment of the GT88 family members and TcdB

GT88 members are *Lpp*GT, *Lppa*GT (*Lp*GT from strain *Paris*), *Lpl*GT, Lgt2 and Lgt3. Secondary structure elements from the *Lpp*GT structure are dark grey for the N-terminal domain, black for the central domain and light grey for the protrusion domain. Conserved catalytic glutamine residues are indicated with a black circle, the aspartic residues of the DxD motif are marked with a black star, amino acids interacting with UDP-glucose by direct hydrogen bonds or hydrophobic stacking interactions are highlighted with a black triangle, and amino acids interacting with UDP-glucose by indirect hydrogen bonds through water molecules are highlighted with a grey triangle.

Europe PMC Funders Author Manuscripts

Europe PMC Funders Author Manuscripts

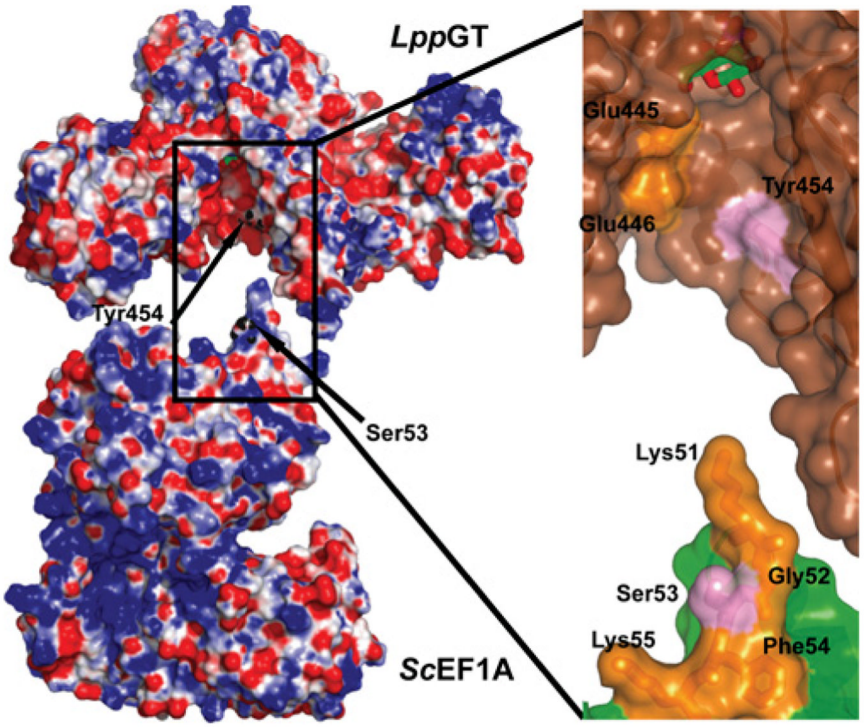

Figure 3. Electrostatic surface representation of *Lpp*GT and *Sc*EF1A

Left-hand panel: *Lpp*GT has a negatively charged binding groove, which may interact with the positively charged loop on *Sc*EF1A (PDB code 2B7B [37]) that carries the acceptor serine. Tyr^{454}, in the putative binding groove on *Lpp*GT, and the acceptor serine (Ser^{53}) on ScEF1A are indicated by arrows. Right-hand panel: higher magnification representation of the putative interaction site between *Lpp*GT and *Sc*EF1A. The surface of *Lpp*GT and *Sc*EF1A are represented in brown and green respectively. Tyr^{454} and Ser^{53} are shown as sticks in pink; charged residues are in yellow (including some other residues forming the loop in which Ser^{53} is localized, such as Gly^{52} and Phe^{54}).

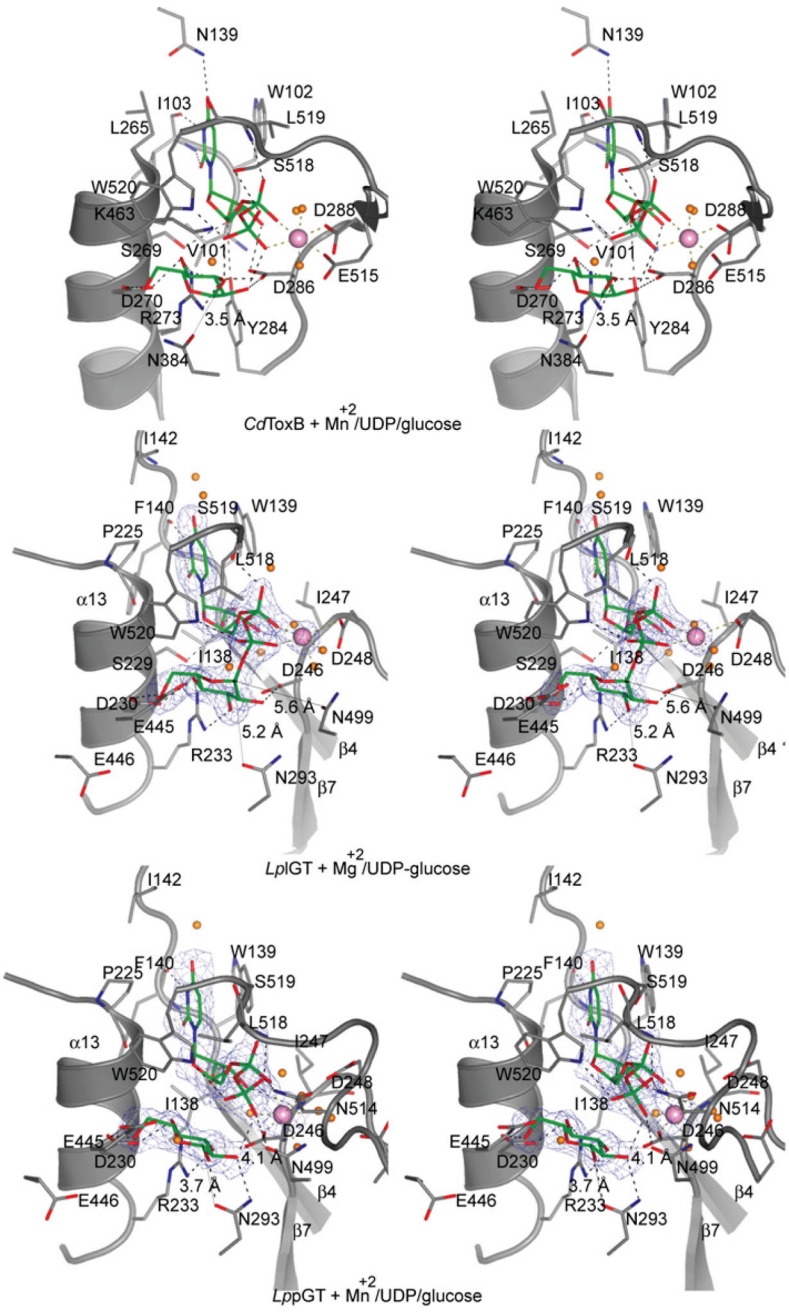

Figure 4. Active site of *Lp*GT bound to UDP-glucose and metals

Stereo images of the *Lpl*GT, *Lpp*GT and TcdB active sites. *Lpl*GT is shown in complex with UDP-glucose and Mg^{2+}. *Lpp*GT and TcdB crystal structures are shown in complex with UDP, glucose and Mn^{2+}. The amino acids are shown as grey sticks. The ligands and metals are shown as green sticks and pink spheres respectively. Protein–ligand hydrogen bonds are shown as broken black lines. The distances between Asn^{293} and Asn^{499} to the anomeric carbon are shown as thin lines. Unbiased (i.e. before inclusion of any inhibitor model) F_o–F_c, ϕ_{calc} electron density maps are shown at 2.5 σ.

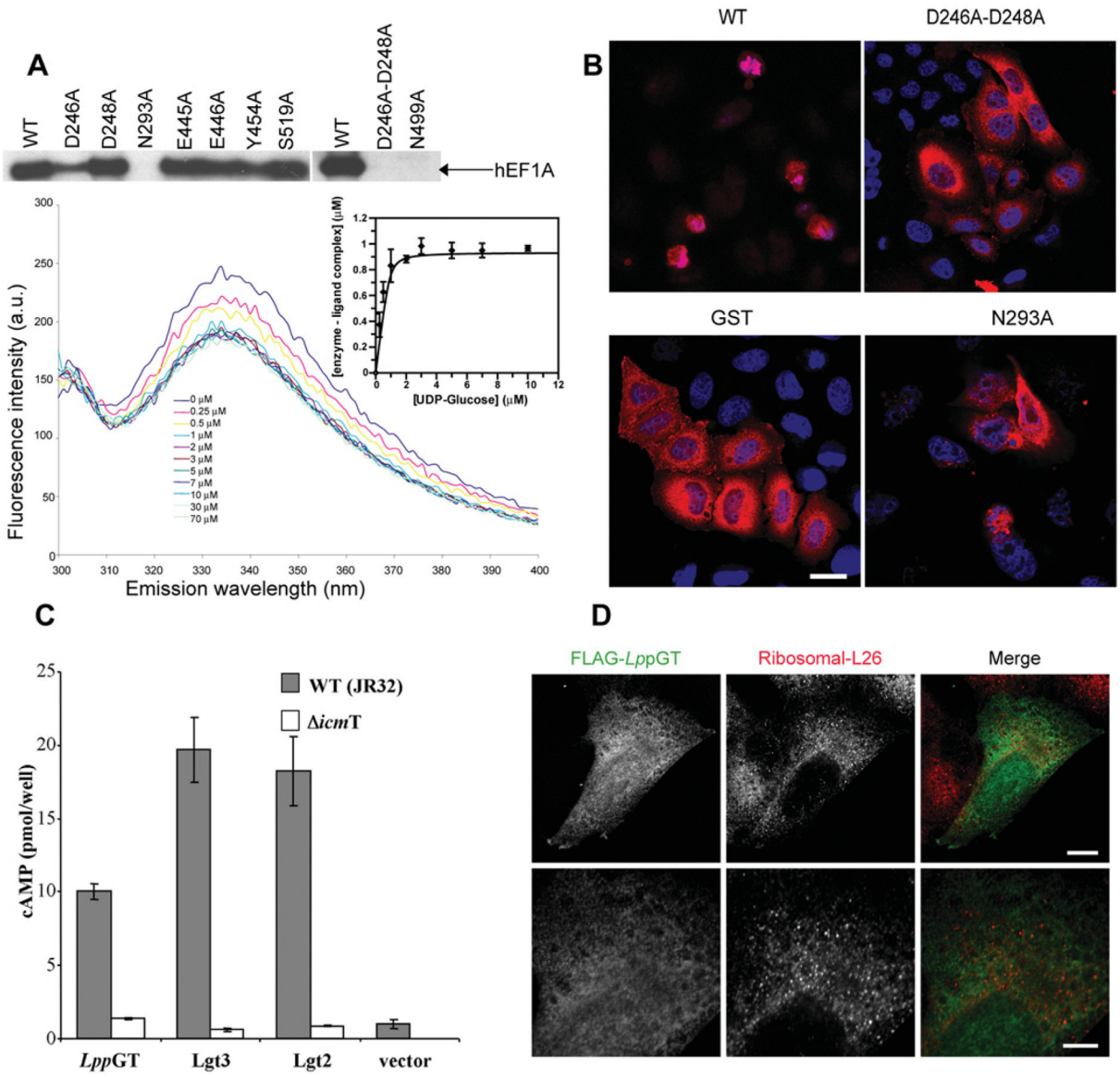

Figure 5. Site-directed mutagenesis, microinjection, translocation and localization studies

(**A**) The upper panel shows autoradiography of wild-type and mutant enzymes incubated with HEK-293 lysates and UDP-[^{3}H]glucose. The lower panel shows quenching of intrinsic *Lpp*GT tryptophan fluorescence measured at increasing concentrations of UDP-glucose. All data points represent the means ± S.D. for three measurements. The K_d for UDP-glucose was determined by fitting fluorescence intensity data against free UDP-glucose concentration (insert). See Table 2 for the K_d values for wild-type and mutant enzymes. (**B**) HeLa cells microinjected with wild-type *Lpp*GT, D246A/D248A double-mutant *Lpp*GT (D246A-D248A), *Lpp*GT-N293A and GST, as a control, at a protein concentration of 30 μM in the injection needle. Cells were co-injected with Texas Red-conjugated dextran and incubated for 48 h and are counterstained with DAPI. Representative images are shown for the cells after 48 h incubation. After injection of wild-type *Lpp*GT, there were few surviving red (Texas-Red–dextran-postive) cells and, of these, most had a rounded-up morphology when compared with cells injected with GST protein and the double mutant *Lpp*GT. *Lpp*GT-N293A was slightly protective compared with the wild-type enzyme. (**C**)

Translocation experiments. All three enzymes were translocated through the Icm/Dot machinery (grey bars) compared with a mutated Δ*icmT Legionella* strain (white bars) as measured by cAMP concentrations. (**D**) Microinjected FLAG-tagged *Lpp*GT protein was injected into HeLa cells and incubated for 24 h. The FLAG-tagged protein (green) was diffusely distributed throughout the cell and showed rare co-localization with the counterstain against ribosomal L26 protein (red). The lower panels show a higher magnification of the image in the upper panels. Scale bar, 10 μm (upper panels) or 5 μm (lower panels). The proteins are FLAG-tagged at the C-terminus.

Europe PMC Funders Author Manuscripts

Table 1
Data collection and refinement statistics

Values in parentheses refer to the highest resolution shell. Ramachandran plot statistics were determined with PROCHECK [25].

Parameter	*Lpl*GT $HgCl_2$ derivative	*Lpl*GT and UDP-glucose	*Lpp*GT, UDP and glucose
Space group	H 3	H 3	P 2_1
Wavelength (Å)	1.003	1.282	1.892
Resolution (Å)	20.0-2.10	20.0-1.9	20.0-2.1
Cell dimensions	*a* = 0122.3Å *b* = 0122.3Å *c* = 103.1Å	*a* = 0122.8Å *b* = 0122.8 *c* = 103.4Å,	*a* = 051.0Å *b* = 0104.6Å *c* = 53.3Å
Unique reflections	33622	45918	31842
Completeness	0.999 (0.991)	0.992 (0.969)	0.971 (0.918)
*R*sym	0.099 (0.520)	0.073 (0.50)	0.125 (0.402)
$I/\sigma(I)$	26.0 (5.7)	29 (5.8)	23.2 (5.5)
Redundancy	12.8 (11.8)	10.3 (7.2)	6.5 (3.6)
R_{work}/R_{free}		0.199/0.261	0.189/0.254
RMSD from ideal geometry, bonds (Å)		0.012	0.008
RMSD from ideal geometry, angles (°)		1.4	1.2
B-factor (backbone bonds) RMSD ($Å^2$)		0.74	0.56
B-factor protein ($Å^2$)		35.4	27.3
B-factor UDP-glucose ($Å^2$)		29.4	
B-factor UDP ($Å^2$)			19.4
B-factor glucose ($Å^2$)			26.9
B-factor solvent ($Å^2$)		40.6	33.5
Ramachandran plot:			
Most favoured (%)		97.7	96.2
Additionally allowed (%)		2.3	2.9
Generously allowed (%)		0.0	0.21
PDB code		2WZG	2WZF

Europe PMC Funders Author Manuscripts

Table 2

Activity and UDP-glucose binding of single- and double-mutants of *Lpp*GT compared with wild-type enzyme

The K_d for UDP-glucose was determined by fitting fluorescence intensity data, obtained by tryptophan fluorescence experiments, against free UDP-glucose concentration (Figure 3A). The activity and K_d experiments results represent means ± S.D. for three independent experiments. The percentage of surviving and intact HeLa cells was determined after 48 h; intact cells were not apoptotic and rounded and represent the mean of two independent experiments. nd, not detectable; –, not performed.

*Lpp*GT varient	% activity	K_d (nM)	% surviving cells	% intact cells
Wild-type	100	100±29	33	10
D246A	48±3	400±80	38	18
D248A	92±3	990±90	36	18
D246A/D248A double-mutant	nd	830±100	100	95
N293A	nd	72±30	93	90
E445A	86±7	41±25	–	–
E446A	78±10	130±40	–	–
Y454A	43±2	60±30	–	–
N499A	nd	90±20	110	110
S519A	87±4	100±43	–	–
GST	–	–	305	300
Buffer	–	–	247	245